Fast Decoupled Multi-energy Flow Calculation for Integrated Energy System

Yanbo Chen, Junyuan Zhao, and Jin Ma

***Abstract*—In recent years, as a promising option to improve the overall efficiency of energy utilization and absorptive capacity of renewable energies, the integrated energy system (IES) has raised great interest in academies and industries. Multi-energy flow (MF) calculation, which differs from the traditional power flow calculation, plays a basic role in analyzing IES. MF calculation based on Newton-Raphson method has been proposed in literature, but its calculation efficiency is not high. In this paper, a fast decoupled MF (FDMF) calculation method for IES is proposed. Its main idea is to replace the original Jacobian matrix of MF calculation based on Newton-Raphson method with a diagonal and constant Jacobian matrix by the transformation. The simulations demonstrate that the proposed FDMF method can increase the calculation efficiency by at least 4 times with high calculation accuracy.**

***Index Terms*—Integrated energy system (IES), multi-energy flow (MF), fast decoupled solution methodology, combined electricity-heat-natural gas system, flow calculation.**

I. Introduction

In recent years, as a promising option to improve the overall efficiency of energy utilization and the absorptive capacity of renewable energies, integrated energy system (IES) has raised great interest in academies and industries. IES integrates the production, storage, transportation, distribution, conversion and consumption of multiple energy sources, i.e., electricity, natural gas, heat/cool, hydrogen supply, etc. Through the comprehensive management and scientific dispatch of multiple energy sources, it can realize the complementary utilization and cascaded utilization of multiple energy sources, so as to meet the diverse needs of users, improve the reliability of social energy supply, improve the overall utilization efficiency of energy system, and ultimately ensure the sustainable development of economy and society.

Multi-energy flow (MF) calculation is the basis of analysis, planning, scheduling and controlling for IES. Since the material properties and MF equations of IES are different from those of power system, traditional calculation method of power flow (PF) cannot be used directly to MF calculation. With the rapid development of IES, in order to realize the rational planning, accurate prediction, accurate decision-making and precise control of IES, it is necessary to study the MF calculation methods.

Most of the current research focuses on the energy flow calculation methods of combined electricity-heat system or combined electricity-natural gas system. Reference [1] proposes an MF calculation method based on Newton-Raphson MF (NRMF) method for combined electricity and heat system. References [2] and [3] investigate the MF calculation method for electricity-heat system, but the two systems are calculated separately and then linked with generating units. References [4]-[8] present a combined operation planning of electricity-natural gas system. Reference [9] presents an MF calculation method of combined electricity-natural gas system and realizes the dynamic modeling. The modeling of the combined coupling components are presented in [10]-[12], including combined heat and power (CHP) units, heat pumps and others. In [13] and [14], an energy hub model of combined electricity-natural gas system is established. However, the above studies cannot realize the coupling and modeling of three systems (electricity, heat and natural gas systems) simultaneously. Therefore, they are also unable to perform MF calculations on the more common IES consisting of power, heat, and natural gas systems.

In [15]-[17], MF calculation method for the combined electricity-heat-natural gas system is presented. In [18] and [19], two approaches for calculating the optimal PF of IES are proposed. In [20], an MF calculation model for IES is presented and solved with NRMF method, thereby laying the foundation for the analysis of IES. In [21], a unified steady-state PF analysis (UMF) considering electricity, natural gas, and district heat networks all together is proposed. However, the defect of the method in [20] and [21] is that the calculation efficiency is not very high, especially for large systems with numerous nodes. The main reason for this drawback is probably ascribed to the high dimension of the integrated Jacobian matrix of MF equations. Besides, the

Manuscript received: September 11, 2018; accepted: November 10, 2019. Date of CrossCheck: November 10, 2019. Date of online publication: August 17, XXXX.

This work was supported in part by the National Natural Science Foundation of China (No. 51777067), in part by the State Key Laboratory of Alternate Electrical Power System with Renewable Energy Sources (No. LAPS2019-08) and in part by the scientific and technological project of State Grid Corporation of China "State Estimation of Integrated Energy Systems Considering Different Time Scales" (No. 52110418002R).

Y. Chen and J. Zhao are with the School of Electrical and Electronic Engineering, North China Electric Power University, Beijing, China (e-mail: yanbochen2008@sina.com; zhaojunyuan2017@sina.com).

J. Ma is with the School of Electrical and Information Engineering, University of Sydney, Sydney, Australia (e-mail: j.ma@sydney.edu.au).

DOI: 10.35833/MPCE.2018.000598

Jacobian matrix of MF equations needs to be formed and factorized in each iteration, which is particularly time-consuming. In order to promote its practicability, it is necessary to further improve the computation efficiency of MF calculation method.

In the electricity system, the fast decoupled PF (FDPF) calculation method [22]-[24] is proposed to improve the calculation efficiency of the basic PF calculation based on NRMF method. A diagonal and constant Jacobian matrix is applied to replace the original Jacobian matrix in PF calculation method according to the characteristics of high-voltage transmission network. Accordingly, we propose a fast decoupled MF (FDMF) calculation method for IES through the in-depth analysis of the characteristics of MF equations and Jacobian matrix. The main idea of the proposed FDMF calculation method is to replace the original Jacobian matrix of MF calculation based on NRMF method with a diagonal and constant Jacobian matrix. We demonstrate that the proposed method can not only ensure the accuracy of calculation, but also greatly improve the efficiency of MF calculation.

The major contributions of this paper are as follows.

1) Through the in-depth analysis of the characteristics of MF equations and the Jacobian matrix of MF calculation method based on NRMF method, the MF equations are decoupled and a diagonal and constant Jacobian matrix is obtained by the transformation.

2) An FDMF calculation method for IES is presented. A large number of simulation experiments demonstrate that the proposed method is effective with high computation efficiency.

The rest of this paper is organized as follows. Section II makes a brief review on modeling of MF calculation for IES. The formulation of FDMF calculation method for IES and the overall calculation procedure are presented in Section III. Case studies on an IES are given in Section IV. Finally, conclusions are drawn in Section V.

II. Brief Review on MF for IES

A. Modeling of MF for IES

1) Modeling of Electricity System

The PF equations of electricity system are described by:

$$\begin{cases} \boldsymbol{P} = \mathrm{Re}\left\{\dot{\boldsymbol{U}}\left(\boldsymbol{Y}\dot{\boldsymbol{U}}\right)^{*}\right\} \\ \boldsymbol{Q} = \mathrm{Im}\left\{\dot{\boldsymbol{U}}\left(\boldsymbol{Y}\dot{\boldsymbol{U}}\right)^{*}\right\} \end{cases} \tag{1}$$

where $\boldsymbol{P}$ and $\boldsymbol{Q}$ are the active and reactive power of node injection, respectively; $\boldsymbol{Y}$ is the node admittance matrix; and $\dot{\boldsymbol{U}}$ is the node complex voltage phasor.

2) Modeling of Heat System

In the heat system, hot water or steam flows in the supply pipes to deliver heat from supply nodes to load nodes, and returns through return pipes. According to its characteristics, the heat system can be divided into two parts: hydraulic model and thermal model.

Hydraulic model is described as: ① the flow of each pipeline should satisfy the flow continuity equation at each node (The mass flow injected into a node minus the mass flow that leaves the node is equal to the flow consumption at the node); ② in a closed loop composed of pipelines, the sum of the pressure variation around a loop is equal to zero. That is:

$$\begin{cases} \boldsymbol{A}_{sl}\boldsymbol{m} = \boldsymbol{m}_{q} \\ \boldsymbol{B}_{h}\boldsymbol{h}_{f} = \boldsymbol{0} \end{cases} \tag{2}$$

where $\boldsymbol{A}_{sl}$ is the node-branch incidence matrix in heat system; $\boldsymbol{m}$ is the mass flow in each pipe; $\boldsymbol{m}_{q}$ is the mass flow injected into the nodes; $\boldsymbol{B}_{h}$ is the loop-branch incidence matrix; and $\boldsymbol{h}_{f}$ is the vector of pressure loss along each pipe and it can be expressed as:

$$\boldsymbol{h}_{f} = \boldsymbol{K}\boldsymbol{m}\left|\boldsymbol{m}\right| \tag{3}$$

where $\boldsymbol{K}$ is the resistance coefficient matrix of pipeline.

The thermal model describes the relationship between the temperature and heat power at each node. The thermal model can be described by:

$$\begin{cases} \boldsymbol{\Phi} = C_{p}\boldsymbol{m}_{q}\left(\boldsymbol{T}_{s} - \boldsymbol{T}_{o}\right) \\ T_{end} = \left(T_{start} - T_{a}\right)\mathrm{e}^{-\frac{\lambda L}{C_{p}m}} + T_{a} \\ \sum m_{out}T_{out} = \sum m_{in}T_{in} \end{cases} \tag{4}$$

where $\boldsymbol{\Phi}$ is the heat power at each node; C_{p} is the specific heat of water; $\boldsymbol{T}_{s}$ is the column vector composed of T_{s} and T_{s} is the supply temperature of hot water entering the load node; $\boldsymbol{T}_{o}$ is the column vector composed of T_{o} and T_{o} is the temperature of hot water flowing out of the load node; T_{end} and T_{start} are the water temperatures at the start and end of each pipe, respectively; T_{a} is the ambient temperature; λ is the heat transfer coefficient; and L is the length of each pipe; m is a scalar representing the mass flow through the current pipeline; m_{out} and T_{out} are the mass flow and temperature of hot water flowing out of the node, respectively; and m_{in} and T_{in} are the mass flow and temperature of water flowing into the node, respectively.

Note that the second and third sub-equations in (4) hold for both the supply heat network and return heat network.

3) Modeling of Gas System

Natural gas model is used to describe the relationship between node pressure and pipeline flow in natural gas network.

The flow continuity equation of natural gas network is:

$$\boldsymbol{A}_{gl}\boldsymbol{f} = \boldsymbol{L} \tag{5}$$

where $\boldsymbol{A}_{gl}$ is the node-branch incidence matrix of natural gas network; $\boldsymbol{f}$ is the natural gas flow in pipeline; and $\boldsymbol{L}$ is the natural gas consumed by nodes.

The calculation method of $\boldsymbol{f}$ is:

$$\boldsymbol{f} = \phi\left(\Delta\Pi_{ij}\right) = K_{r}s_{ij}\sqrt{s_{ij}\left(\Pi_{i} - \Pi_{j}\right)} \tag{6}$$

where ϕ is the symbol of the function; $\Delta\Pi_{ij}$ is the pressure drop of the pipe ij and $\Delta\Pi_{ij} = \Pi_{i} - \Pi_{j}$; Π_{i} and Π_{j} are the pressures of node i and node j, respectively; K_{r} is the pipe coefficient; and s_{ij} is equal to +1 when the natural gas flow runs

from i to j, otherwise $s_{ij}=-1$.

Pressure drop vectors of all natural gas pipelines $\Delta\boldsymbol{\Pi}$ can be expressed as:

$$\Delta\boldsymbol{\Pi}=-\boldsymbol{A}_{gl}^{\mathrm{T}}\boldsymbol{\Pi} \tag{7}$$

where $\boldsymbol{\Pi}$ is the vector consisting of Π_i.

B. MF Equations for IES

For the IES consisting of electricity, heat and natural gas systems, the MF equations can be described as [20]:

$$\Delta\boldsymbol{F}(\boldsymbol{x})=\begin{bmatrix}\Delta\boldsymbol{F}_e\\ \Delta\boldsymbol{F}_h\\ \Delta\boldsymbol{F}_g\end{bmatrix}=\begin{bmatrix}\Delta\boldsymbol{P}\\ \Delta\boldsymbol{Q}\\ \Delta\boldsymbol{\Phi}\\ \Delta\boldsymbol{p}\\ \Delta\boldsymbol{T}_s\\ \Delta\boldsymbol{T}_r\\ \Delta\boldsymbol{f}\end{bmatrix}=\begin{bmatrix}\boldsymbol{P}^{SP}-\mathrm{Re}\left\{\dot{\boldsymbol{U}}\left(\boldsymbol{Y}\dot{\boldsymbol{U}}\right)^*\right\}\\ \boldsymbol{Q}^{SP}-\mathrm{Im}\left\{\dot{\boldsymbol{U}}\left(\boldsymbol{Y}\dot{\boldsymbol{U}}\right)^*\right\}\\ C_p\boldsymbol{A}_{sl}\boldsymbol{m}\left(\boldsymbol{T}_s-\boldsymbol{T}_o\right)-\boldsymbol{\Phi}\\ \boldsymbol{B}_h\boldsymbol{K}\boldsymbol{m}|\boldsymbol{m}|\\ \boldsymbol{C}_s\boldsymbol{T}_{s,load}-\boldsymbol{b}_s\\ \boldsymbol{C}_r\boldsymbol{T}_{r,load}-\boldsymbol{b}_r\\ \boldsymbol{A}_{gl}\phi\left(-\boldsymbol{A}_{gl}^{\mathrm{T}}\boldsymbol{\Pi}\right)-\boldsymbol{L}\end{bmatrix}=\boldsymbol{0} \tag{8}$$

where Δ represents the imbalance; the subscripts e, h, and g represent the electricity system, heat system and natural gas system, respectively; $\boldsymbol{p}$ is the sum of the pressure changes around the loops; $\boldsymbol{P}^{SP}$ and $\boldsymbol{Q}^{SP}$ are the injection active vector and the injection reactive vector of the node, respectively; $\boldsymbol{T}_r$ is the column vector composed of T_r and T_r is the return temperature of hot water; $\boldsymbol{C}_s$ and $\boldsymbol{C}_r$ are the matrices related to the structure and mass flow of heat network and regenerative network, respectively; $\boldsymbol{b}_s$ and $\boldsymbol{b}_r$ are the column vectors related to heat temperature and output temperature, respectively; $\boldsymbol{T}_{s,load}$ is the column vector composed of $T_{s,load}$ and $T_{s,load}=T_s-T_a$; and $\boldsymbol{T}_{r,load}$ is the column vector composed of $T_{s,load}$ and $T_{r,load}=T_r-T_a$.

And $\boldsymbol{x}$ in (8) is given by:

$$\boldsymbol{x}=\begin{bmatrix}\boldsymbol{x}_e^{\mathrm{T}} & \boldsymbol{x}_h^{\mathrm{T}} & \boldsymbol{x}_g^{\mathrm{T}}\end{bmatrix}^{\mathrm{T}}=\begin{bmatrix}\boldsymbol{\theta}^{\mathrm{T}} & \boldsymbol{U}^{\mathrm{T}} & \boldsymbol{m}^{\mathrm{T}} & \boldsymbol{T}_{s,load}^{\mathrm{T}} & \boldsymbol{T}_{r,load}^{\mathrm{T}} & \boldsymbol{\Pi}^{\mathrm{T}}\end{bmatrix}^{\mathrm{T}} \tag{9}$$

where $\boldsymbol{\theta}$ is the phase angle vector of all nodes except the reference node; and $\boldsymbol{U}$ is the voltage amplitude vector of all nodes.

The calculation method of $\boldsymbol{b}_s$ and $\boldsymbol{b}_r$ is given in [1]. More details of MF equations can be found in [20].

C. Solution of MF Equations Based on NRMF Method

As can be seen in (8), the MF equations of IES are nonlinear algebraic equations, which are suitable to be solved with NRMF method [20]. Its iteration equations are given by:

$$\begin{cases}\Delta\boldsymbol{F}^{(k)}=\boldsymbol{J}^{(k)}\Delta\boldsymbol{x}^{(\mathrm{k}+1)}\\ \boldsymbol{x}^{(k+1)}=\boldsymbol{x}^{(k)}-\Delta\boldsymbol{x}^{(k)}\end{cases} \tag{10}$$

where k is the iterative counter; and $\boldsymbol{J}$ is the Jacobian matrix.

After several iterations until $\left\|\Delta\boldsymbol{x}^{(k)}\right\|\le\varepsilon$, the solution of $\boldsymbol{x}$ can be obtained, where ε is the accuracy.

From the above solution process, we can find that the main computation burden of NRMF lies in that the Jacobian matrix needs to be re-calculated and refactorized in each iteration, which is time-consuming. Motivated by the fast decoupled method for electric PF calculation, we propose an FDMF calculation method for IES. The main idea is to replace the original Jacobian matrix with a diagonalized and constant Jacobian matrix. We demonstrate that the proposed method can greatly enhance the efficiency of MF calculation.

III. FDMF Calculation Method for IES

A. Jacobian Matrix of Combined Network

$\boldsymbol{J}$ in (10) can be expressed as:

$$\boldsymbol{J}=\begin{bmatrix}\boldsymbol{J}_{ee} & \boldsymbol{J}_{eh} & \boldsymbol{J}_{eg}\\ \boldsymbol{J}_{he} & \boldsymbol{J}_{hh} & \boldsymbol{J}_{hg}\\ \boldsymbol{J}_{ge} & \boldsymbol{J}_{gh} & \boldsymbol{J}_{gg}\end{bmatrix}=\begin{bmatrix}\frac{\partial\Delta\boldsymbol{F}_e}{\partial\boldsymbol{x}_e^{\mathrm{T}}} & \frac{\partial\Delta\boldsymbol{F}_e}{\partial\boldsymbol{x}_h^{\mathrm{T}}} & \frac{\partial\Delta\boldsymbol{F}_e}{\partial\boldsymbol{x}_g^{\mathrm{T}}}\\ \frac{\partial\Delta\boldsymbol{F}_h}{\partial\boldsymbol{x}_e^{\mathrm{T}}} & \frac{\partial\Delta\boldsymbol{F}_h}{\partial\boldsymbol{x}_h^{\mathrm{T}}} & \frac{\partial\Delta\boldsymbol{F}_h}{\partial\boldsymbol{x}_g^{\mathrm{T}}}\\ \frac{\partial\Delta\boldsymbol{F}_g}{\partial\boldsymbol{x}_e^{\mathrm{T}}} & \frac{\partial\Delta\boldsymbol{F}_g}{\partial\boldsymbol{x}_h^{\mathrm{T}}} & \frac{\partial\Delta\boldsymbol{F}_g}{\partial\boldsymbol{x}_g^{\mathrm{T}}}\end{bmatrix} \tag{11}$$

where the three diagonal blocks represent the partial derivatives of each sub-system to its own state variables; the other six off-diagonal blocks represent the partial derivatives of each sub-system to the state variables of the other systems. All the nine blocks are derived and analyzed below.

1) Expression of $\boldsymbol{J}_{ee}$

The expression of the diagonal block $\boldsymbol{J}_{ee}$ is the same as in the traditional electric system:

$$\boldsymbol{J}_{ee}=\begin{bmatrix}\boldsymbol{H} & \boldsymbol{N}\\ \boldsymbol{K} & \boldsymbol{L}\end{bmatrix}=\begin{bmatrix}\frac{\partial\Delta\boldsymbol{P}}{\partial\boldsymbol{\theta}} & \frac{\partial\Delta\boldsymbol{P}}{\partial\boldsymbol{U}}\\ \frac{\partial\Delta\boldsymbol{Q}}{\partial\boldsymbol{\theta}} & \frac{\partial\Delta\boldsymbol{Q}}{\partial\boldsymbol{U}}\end{bmatrix} \tag{12}$$

where $\boldsymbol{H}=\partial\Delta\boldsymbol{P}/\partial\boldsymbol{\theta}$ is the derivative of the active imbalance with respect to the phase angle vector; $\boldsymbol{N}=\partial\Delta\boldsymbol{P}/\partial\boldsymbol{U}$ is the derivative of the active imbalance to the voltage magnitude vector; $\boldsymbol{K}=\partial\Delta\boldsymbol{Q}/\partial\boldsymbol{\theta}$; and $\boldsymbol{L}=\partial\Delta\boldsymbol{Q}/\partial\boldsymbol{U}$.

For IES, experiments show that $\boldsymbol{J}_{ee}$ does not change much during the iteration process, so $\boldsymbol{J}_{ee}$ can be approximated as a constant matrix evaluated at the flat start.

2) Expression of $\boldsymbol{J}_{hh}$

The expression of the diagonal block $\boldsymbol{J}_{hh}$ is given by:

$$\boldsymbol{J}_{hh}=\begin{bmatrix}\frac{\partial\Delta\boldsymbol{\Phi}}{\partial\boldsymbol{m}^{\mathrm{T}}} & \frac{\partial\Delta\boldsymbol{\Phi}}{\partial\boldsymbol{T}_{s,load}^{\mathrm{T}}} & \frac{\partial\Delta\boldsymbol{\Phi}}{\partial\boldsymbol{T}_{r,load}^{\mathrm{T}}}\\ \frac{\partial\Delta\boldsymbol{p}}{\partial\boldsymbol{m}^{\mathrm{T}}} & \frac{\partial\Delta\boldsymbol{p}}{\partial\boldsymbol{T}_{s,load}^{\mathrm{T}}} & \frac{\partial\Delta\boldsymbol{p}}{\partial\boldsymbol{T}_{r,load}^{\mathrm{T}}}\\ \frac{\partial\Delta\boldsymbol{T}_s}{\partial\boldsymbol{m}^{\mathrm{T}}} & \frac{\partial\Delta\boldsymbol{T}_s}{\partial\boldsymbol{T}_{s,load}^{\mathrm{T}}} & \frac{\partial\Delta\boldsymbol{T}_s}{\partial\boldsymbol{T}_{r,load}^{\mathrm{T}}}\\ \frac{\partial\Delta\boldsymbol{T}_r}{\partial\boldsymbol{m}^{\mathrm{T}}} & \frac{\partial\Delta\boldsymbol{T}_r}{\partial\boldsymbol{T}_{s,load}^{\mathrm{T}}} & \frac{\partial\Delta\boldsymbol{T}_r}{\partial\boldsymbol{T}_{r,load}^{\mathrm{T}}}\end{bmatrix}=\begin{bmatrix}\boldsymbol{J}_{h11} & \boldsymbol{J}_{h12}\\ \boldsymbol{J}_{h21} & \boldsymbol{J}_{h22}\end{bmatrix} \tag{13}$$

The expressions of each sub-block in $\boldsymbol{J}_{hh}$ are derived as:

$$\boldsymbol{J}_{h11}=\begin{bmatrix}\frac{\partial\Delta\boldsymbol{\Phi}}{\partial\boldsymbol{m}^{\mathrm{T}}}\\ \frac{\partial\Delta\boldsymbol{p}}{\partial\boldsymbol{m}^{\mathrm{T}}}\end{bmatrix}=\begin{bmatrix}C_p\cdot\mathrm{diag}\left\{\boldsymbol{T}_s-\boldsymbol{T}_o\right\}\cdot\boldsymbol{A}_{sl}\\ 2\boldsymbol{B}_h\boldsymbol{K}|\boldsymbol{m}|\end{bmatrix} \tag{14}$$

$$\boldsymbol{J}_{h12}=\begin{bmatrix}\dfrac{\partial\Delta\boldsymbol{\Phi}}{\partial\boldsymbol{T}_{s,load}^{\mathrm{T}}} & \dfrac{\partial\Delta\boldsymbol{\Phi}}{\partial\boldsymbol{T}_{r,load}^{\mathrm{T}}}\\ \dfrac{\partial\Delta\boldsymbol{p}}{\partial\boldsymbol{T}_{s,load}^{\mathrm{T}}} & \dfrac{\partial\Delta\boldsymbol{p}}{\partial\boldsymbol{T}_{s,load}^{\mathrm{T}}}\end{bmatrix}=\begin{bmatrix}C_p\cdot\mathrm{diag}\left\{\boldsymbol{A}_{sl}\boldsymbol{m}\right\} & \boldsymbol{0}\\ \boldsymbol{0} & \boldsymbol{0}\end{bmatrix} \tag{15}$$

$$\boldsymbol{J}_{h21}=\begin{bmatrix}\dfrac{\partial\Delta\boldsymbol{T}_s}{\partial\boldsymbol{m}^{\mathrm{T}}}\\ \dfrac{\partial\Delta\boldsymbol{T}_r}{\partial\boldsymbol{m}^{\mathrm{T}}}\end{bmatrix}=\begin{bmatrix}-\dfrac{\partial b_s}{\partial\boldsymbol{m}^{\mathrm{T}}}\\ -\dfrac{\partial b_r}{\partial\boldsymbol{m}^{\mathrm{T}}}\end{bmatrix} \tag{16}$$

$$\boldsymbol{J}_{h22}=\begin{bmatrix}\dfrac{\partial\Delta\boldsymbol{T}_s}{\partial\boldsymbol{T}_{s,load}^{\mathrm{T}}} & \dfrac{\partial\Delta\boldsymbol{T}_s}{\partial\boldsymbol{T}_{r,load}^{\mathrm{T}}}\\ \dfrac{\partial\Delta\boldsymbol{T}_r}{\partial\boldsymbol{T}_{s,load}^{\mathrm{T}}} & \dfrac{\partial\Delta\boldsymbol{T}_r}{\partial\boldsymbol{T}_{s,load}^{\mathrm{T}}}\end{bmatrix}=\begin{bmatrix}\boldsymbol{C}_s & \boldsymbol{0}\\ \boldsymbol{0} & \boldsymbol{C}_r\end{bmatrix} \tag{17}$$

The elements in $\boldsymbol{J}_{h21}$ denote the partial derivative of the mixing temperature at the node of the heat and regenerative network to the mass flow of water in the pipeline. Generally speaking, compared with other non-zero elements of $\boldsymbol{J}$, the elements in $\boldsymbol{J}_{h21}$ are very small and negligible. This has been verified by Section IV-A and many other simulation experiments, hence we have $\boldsymbol{J}_{h21}=\boldsymbol{0}$.

The procedures to form the matrices $\boldsymbol{C}_s$ and $\boldsymbol{C}_r$ are illustrated in [1]. In a typical two-node system, the expressions of $\boldsymbol{C}_s$ and $\boldsymbol{C}_r$ are:

$$\boldsymbol{C}_s=\begin{bmatrix}1 & 0\\ -m_2\Psi_2 & m_1\end{bmatrix} \tag{18}$$

$$\boldsymbol{C}_r=\begin{bmatrix}m_1 & -m_2\Psi_2\\ 0 & 1\end{bmatrix} \tag{19}$$

where $\Psi_2=\exp\left(-\lambda L/\left(C_p m_2\right)\right)$; and $m_i\,(i=1,2)$ denotes the mass flow in the i^{th} pipe of the heat network.

As can be seen from (18) and (19), $\boldsymbol{C}_s$ and $\boldsymbol{C}_r$ should be updated in each iteration as they contain the state variables; and the coefficient Ψ_2 in $\boldsymbol{C}_s$ and $\boldsymbol{C}_r$ is also related to the temperature drop along a pipe. As a result, $\boldsymbol{J}_{hh}$ is non-constant but highly sparse.

3) Expression of $\boldsymbol{J}_{gg}$

The expression of the diagonal block $\boldsymbol{J}_{gg}$ is given by:

$$\boldsymbol{J}_{gg}=\frac{\partial\Delta\boldsymbol{f}}{\partial\boldsymbol{\Pi}}=\boldsymbol{A}_{gl}\boldsymbol{D}\boldsymbol{A}_{gl}^{\mathrm{T}} \tag{20}$$

where $\boldsymbol{D}$ is a diagonal matrix and its i^{th} diagonal element is given by $d_{ii}=f_i/\left(2\Delta\Pi_i\right)$.

4) Expressions of $\boldsymbol{J}_{eg}$, $\boldsymbol{J}_{hg}$, $\boldsymbol{J}_{he}$, and $\boldsymbol{J}_{ge}$

In the IES, natural gas source is connected to the slack bus and the fluctuation of natural gas network can be offset by the change of natural gas supply at the slack bus [20]. Therefore, the electricity and the heat networks are not affected by natural gas fluctuation, and the sub-matrices $\boldsymbol{J}_{eg}$ and $\boldsymbol{J}_{hg}$ are null matrices [20]. Similarly, the fluctuation of the electricity network can be balanced by the grid, so $\boldsymbol{J}_{he}$ and $\boldsymbol{J}_{ge}$ are also null matrices.

5) Expressions of $\boldsymbol{J}_{eh}$ and $\boldsymbol{J}_{gh}$

The slack bus of the heat system is usually connected to the CHP unit, whose working mode usually determines the electric load by thermal load. When the state of the heat system changes, the fluctuation of thermal power produced by CHP unit at slack bus will simultaneously affect the electric power and natural gas consumption, so $\boldsymbol{J}_{eh}$ and $\boldsymbol{J}_{gh}$ are non-zero matrices. Note that the fluctuation of thermal power of other nodes will not affect the electric power and natural gas consumption. Hence, only the rows corresponding to the node connected with CHP units have non-zero elements, and the other elements are still zero elements.

The thermal power $\boldsymbol{\Phi}_{CHP}$, electric power $\boldsymbol{P}_{CHP}^{sp}$ and the natural gas consumption $\boldsymbol{F}_{CHP}$ of CHP unit at slack bus are:

$$\begin{cases}\boldsymbol{\Phi}_{CHP}=C_p\boldsymbol{A}_{sl,CHP}\boldsymbol{m}_{CHP}\left(\boldsymbol{T}_{s,CHP}-\boldsymbol{T}_{o,CHP}\right)\\ \boldsymbol{P}_{CHP}^{sp}=\dfrac{\boldsymbol{\Phi}_{CHP}}{c_m}\\ \boldsymbol{F}_{CHP}=\dfrac{\boldsymbol{\Phi}_{CHP}}{c_m\eta_e}\end{cases} \tag{21}$$

where $\boldsymbol{A}_{sl,CHP}$ is the row corresponding to CHP units in node-branch incidence matrix of thermal system; $\boldsymbol{T}_{s,CHP}$ and $\boldsymbol{T}_{o,CHP}$ are the column vectors composed of elements corresponding to CHP in vectors $\boldsymbol{T}_s$ and $\boldsymbol{T}_o$, respectively; c_m is the thermoelectric scaling factor of the CHP unit; and η_e is related to the electric power produced by the CHP unit.

According to (21), $\boldsymbol{J}_{eh}$ and $\boldsymbol{J}_{gh}$ can be obtained as:

$$\boldsymbol{J}_{eh}=\mathrm{diag}\left\{\boldsymbol{T}_{s,CHP}-\boldsymbol{T}_{o,CHP}\right\}\boldsymbol{A}_{sl,CHP}/c_m \tag{22}$$

$$\boldsymbol{J}_{gh}=-\mathrm{diag}\left\{\boldsymbol{T}_{s,CHP}-\boldsymbol{T}_{o,CHP}\right\}\boldsymbol{A}_{sl,CHP}/\left(c_m\eta_e\right) \tag{23}$$

According to the above deduction process, it can be found that: ① $\boldsymbol{J}$ in (11) is a sparse matrix, but not a constant matrix; ② in the six non-diagonal block matrices of $\boldsymbol{J}$, two are not zero matrices. Therefore, it is impossible to decouple MF calculation directly.

B. Decoupling of MF Equations

1) Decoupling Modeling of Electricity System

According to the above analysis, the corresponding elements in $\boldsymbol{J}_{eh}$ are 0 for electric nodes that are not connected with CHP units, while the corresponding elements in $\boldsymbol{J}_{eh}$ are not 0 for electric nodes connected with CHP units. Therefore, the modeling of the electric power equations should be differentiated whether the node is connected with CHP units or not.

1) For the electric nodes which are not connected with CHP units, $\Delta\boldsymbol{F}_e$ is only related to $\Delta\boldsymbol{x}_e$, then we have:

$$\Delta\boldsymbol{F}_e=\begin{bmatrix}\Delta\boldsymbol{P}\\ \Delta\boldsymbol{Q}\end{bmatrix}=\boldsymbol{J}_{ee}\Delta\boldsymbol{x}_e=\begin{bmatrix}\boldsymbol{H} & \boldsymbol{N}\\ \boldsymbol{K} & \boldsymbol{L}\end{bmatrix}\begin{bmatrix}\Delta\boldsymbol{\theta}\\ \Delta\boldsymbol{U}\end{bmatrix} \tag{24}$$

In IES (power system is often medium- and low-voltage distribution network), the network parameters or operation conditions violate the decoupling conditions applicable to transmission systems, especially for ultra-high-voltage and high-voltage transmission systems. Hence, $\boldsymbol{P}$ and $\boldsymbol{Q}$ in IES cannot be decoupled directly.

In order to solve this problem, we have pointed out that for PQ nodes, $P_i+Q_iG_{ii}/B_{ii}$ can be regarded as quasi active

power, $-P_i G_{ii}/B_{ii}+Q_i$ can be regarded as quasi reactive power, and they have good decoupling properties for different systems even for the distribution with large ratio of resistance to reactance (R/X) in [25]. Therefore, for the i^{th} real and reactive power of the electricity system in IES, the following decoupling correction equations can be adopted for PQ nodes:

$$\begin{bmatrix} \Delta P_i+\dfrac{G_{ii}}{B_{ii}}\Delta Q_i \\ -\dfrac{G_{ii}}{B_{ii}}\Delta P_i+\Delta Q_i \end{bmatrix}=\begin{bmatrix} \boldsymbol{H}_i+\dfrac{G_{ii}}{B_{ii}}\boldsymbol{K}_i & \boldsymbol{0} \\ \boldsymbol{0} & -\dfrac{G_{ii}}{B_{ii}}\boldsymbol{N}_i+\boldsymbol{L}_i \end{bmatrix}\begin{bmatrix} \Delta\boldsymbol{\theta} \\ \Delta\boldsymbol{U} \end{bmatrix} \tag{25}$$

where $\boldsymbol{H}_i$, $\boldsymbol{K}_i$, $\boldsymbol{N}_i$, and $\boldsymbol{L}_i$ are the corresponding rows of $\boldsymbol{H}$, $\boldsymbol{K}$, $\boldsymbol{N}$, and $\boldsymbol{L}$, respectively. The coefficient matrices are constant. Details can be found in [25].

For PV nodes, only the active power is given, at this time we have:

$$\Delta P_i=\begin{bmatrix}\boldsymbol{H}_i & \boldsymbol{N}_i\end{bmatrix}\begin{bmatrix}\Delta\boldsymbol{\theta} \\ \Delta\boldsymbol{U}\end{bmatrix} \tag{26}$$

Equation (26) can be further transformed into the following decoupled form with constant Jacobian matrices:

$$\Delta P_i-\boldsymbol{N}_i\Delta\boldsymbol{U}=\boldsymbol{H}_i\Delta\boldsymbol{\theta} \tag{27}$$

The coefficient matrices are also constant. Details can be found in [25].

2) For the electric nodes connected with CHP units, the active power of CHP unit is given by (21), that is:

$$\boldsymbol{P}_{CHP}^{sp}=C_p\boldsymbol{A}_{sl,CHP}\boldsymbol{m}_{CHP}\left(\boldsymbol{T}_{s,CHP}-\boldsymbol{T}_{o,CHP}\right)/c_m \tag{28}$$

The active power equation corresponding to CHP unit is:

$$\Delta\boldsymbol{P}_{CHP}=C_p\boldsymbol{A}_{sl,CHP}\boldsymbol{m}_{CHP}\left(\boldsymbol{T}_{s,CHP}-\boldsymbol{T}_{o,CHP}\right)/c_m-\mathrm{Re}\left\{\dot{\boldsymbol{U}}_{CHP}(\boldsymbol{Y}\dot{\boldsymbol{U}})^*\right\}=\boldsymbol{0} \tag{29}$$

The correction equation for CHP unit is given by:

$$\Delta\boldsymbol{P}_{CHP}=\boldsymbol{J}_{ee}\Delta\boldsymbol{x}_e+\boldsymbol{J}_{eh}\Delta\boldsymbol{m}=\begin{bmatrix}\boldsymbol{H}_{i,CHP} & \boldsymbol{N}_{i,CHP}\end{bmatrix}\begin{bmatrix}\Delta\boldsymbol{\theta} \\ \Delta\boldsymbol{U}\end{bmatrix}+\mathrm{diag}\left\{\boldsymbol{T}_{s,CHP}-\boldsymbol{T}_{o,CHP}\right\}\boldsymbol{A}_{sl,CHP}/c_m\Delta\boldsymbol{m} \tag{30}$$

Equation (30) can be further transformed into the following decoupled form with constant Jacobian matrices:

$$\Delta\boldsymbol{P}_{CHP}-\mathrm{diag}\left\{\boldsymbol{T}_{s,CHP}-\boldsymbol{T}_{o,CHP}\right\}\boldsymbol{A}_{sl,CHP}/c_m\Delta\boldsymbol{m}-\boldsymbol{N}_{i,CHP}\Delta\boldsymbol{U}=\boldsymbol{H}_{i,CHP}\Delta\boldsymbol{\theta} \tag{31}$$

2) Decoupling Modeling of Heat System

It should be pointed out that heat networks are typically radial rather than meshed to reduce investments and heat losses as well as assure the flexibility when adding new heat load nodes due to the uncertainty of urban development. Communicating pipes are used to improve the reliability, whose valves are only open under fault conditions. Such design is the most accepted in actual engineering. For simplicity, this paper only considers the heat networks without meshes.

For radial heat networks, the equation $\boldsymbol{B}_h\boldsymbol{K}\boldsymbol{m}|\boldsymbol{m}|=\boldsymbol{0}$ does not exist and is not included in MF equations. The corresponding Jacobian sub-blocks should also be deleted from $\boldsymbol{J}_{h11}$ and $\boldsymbol{J}_{h12}$ in (13).

Since $\boldsymbol{J}_{he}$ and $\boldsymbol{J}_{hg}$ are zero matrices, the unbalance of the heat system is only related to the deviation of its own state variables, that is:

$$\Delta\boldsymbol{F}_h=\begin{bmatrix}\Delta\boldsymbol{\Phi} \\ \Delta\boldsymbol{T}_s \\ \Delta\boldsymbol{T}_r\end{bmatrix}=\boldsymbol{J}_{hh}\begin{bmatrix}\Delta m \\ \Delta\boldsymbol{T}_{s,load} \\ \Delta\boldsymbol{T}_{r,load}\end{bmatrix} \tag{32}$$

Substituting $\boldsymbol{J}_{hh}$ in (13) into (8) and ignore the rows corresponding to $\Delta\boldsymbol{p}=\boldsymbol{B}_h\boldsymbol{K}\boldsymbol{m}|\boldsymbol{m}|=\boldsymbol{0}$, we can get:

$$\begin{bmatrix}\Delta\boldsymbol{\Phi} \\ \Delta\boldsymbol{T}_s \\ \Delta\boldsymbol{T}_r\end{bmatrix}=\begin{bmatrix} C_p\cdot\mathrm{diag}\left\{\boldsymbol{T}_s-\boldsymbol{T}_o\right\}\cdot\boldsymbol{A}_{sl} & C_p\cdot\mathrm{diag}\left\{\boldsymbol{A}_{sl}\boldsymbol{m}\right\} & \boldsymbol{0} \\ \boldsymbol{0} & \boldsymbol{C}_s & \boldsymbol{0} \\ \boldsymbol{0} & \boldsymbol{0} & \boldsymbol{C}_r \end{bmatrix}\cdot\begin{bmatrix}\Delta m \\ \Delta\boldsymbol{T}_{s,load} \\ \Delta\boldsymbol{T}_{r,load}\end{bmatrix} \tag{33}$$

Equation (33) can be transformed into:

$$\begin{cases}\Delta\boldsymbol{\Phi}-C_p\cdot\mathrm{diag}\left\{\boldsymbol{A}_{sl}\boldsymbol{m}\right\}\cdot\Delta\boldsymbol{T}_{s,load}=C_p\cdot\mathrm{diag}\left\{\boldsymbol{T}_s-\boldsymbol{T}_o\right\}\cdot\boldsymbol{A}_{sl}\Delta\boldsymbol{m} \\ \Delta\boldsymbol{T}_s=\boldsymbol{C}_s\Delta\boldsymbol{T}_{s,load} \\ \Delta\boldsymbol{T}_r=\boldsymbol{C}_r\Delta\boldsymbol{T}_{r,load}\end{cases} \tag{34}$$

Although (34) has decoupling form, their Jacobian coefficient matrices are not constant. This can be solved in the following ways: ① multiplying left by $\left(\mathrm{diag}\left\{\boldsymbol{T}_s-\boldsymbol{T}_o\right\}\right)^{-1}$ on both sides of the first sub-equation in (34), then a constant Jacobian coefficient matrix can be obtained; ② in IES, a large number of experiments show that the values of $\boldsymbol{C}_s$ and $\boldsymbol{C}_r$ do not change much during the iteration process, so $\boldsymbol{C}_s$ and $\boldsymbol{C}_r$ can be approximated as constant matrices evaluated at the flat start. Then we can get the heat system equations in decoupled form with constant Jacobi matrices:

$$\begin{cases}\left(\mathrm{diag}\left\{\boldsymbol{T}_s-\boldsymbol{T}_o\right\}\right)^{-1}\left(\Delta\boldsymbol{\Phi}-C_p\cdot\mathrm{diag}\left\{\boldsymbol{A}_{sl}\boldsymbol{m}\right\}\cdot\Delta\boldsymbol{T}_{s,load}\right)=C_p\boldsymbol{A}_{sl}\Delta\boldsymbol{m} \\ \Delta\boldsymbol{T}_s=\boldsymbol{C}_s^{(0)}\Delta\boldsymbol{T}_{s,load} \\ \Delta\boldsymbol{T}_r=\boldsymbol{C}_r^{(0)}\Delta\boldsymbol{T}_{r,load}\end{cases} \tag{35}$$

where $\boldsymbol{C}_s^{(0)}$ and $\boldsymbol{C}_r^{(0)}$ are the values of $\boldsymbol{C}_s$ and $\boldsymbol{C}_r$ in the first iteration, respectively.

3) Decoupling Modeling of Natural Gas System

For natural gas systems, according to (11), we have the following correction equations:

$$\Delta\boldsymbol{f}=\boldsymbol{J}_{gh}\Delta\boldsymbol{x}_h+\boldsymbol{J}_{gg}\Delta\boldsymbol{x}_g=\left[-\mathrm{diag}\left\{\boldsymbol{T}_{s,CHP}-\boldsymbol{T}_{o,CHP}\right\}\cdot\boldsymbol{A}_{sl,CHP}/\left(c_m\eta_e\right)\Delta\boldsymbol{m}\right]+\boldsymbol{A}_{gl}\boldsymbol{D}\boldsymbol{A}_{gl}^{\mathrm{T}}\Delta\boldsymbol{\Pi} \tag{36}$$

Equation (36) can be transformed into the following decoupled form with constant Jacobian matrices:

$$\Delta\boldsymbol{f}+\left[\mathrm{diag}\left\{\boldsymbol{T}_{s,CHP}-\boldsymbol{T}_{o,CHP}\right\}\cdot\boldsymbol{A}_{sl,CHP}/\left(c_m\eta_e\right)\right]\Delta\boldsymbol{m}=\boldsymbol{A}_{gl}\boldsymbol{D}\boldsymbol{A}_{gl}^{\mathrm{T}}\Delta\boldsymbol{\Pi} \tag{37}$$

C. Overall Algorithm

By the transformations given above, the MF equations of IES are decoupled. These decoupled equations can be solved quickly by forward-backward method until they converge. The calculation procedure can be summarized in Algorithm 1.

Algorithm 1: FDMF

1: (initialization) let $\boldsymbol{x}^{(0)}$ be the flat start state variables. Set the convergence tolerance $\varepsilon=10^{-3}$. Set the iteration count k=0.
2: calculate all the constant Jacobian matrices.
3: solve (25), (27) and (31) for $\left[\Delta\boldsymbol{\theta}^{\mathrm{T}},\Delta\boldsymbol{U}^{\mathrm{T}}\right]^{\mathrm{T}}$; solve (35) for $\left[\Delta\boldsymbol{m}^{\mathrm{T}},\Delta\boldsymbol{T}_{s,load}^{\mathrm{T}},\Delta\boldsymbol{T}_{r,load}^{\mathrm{T}}\right]^{\mathrm{T}}$; solve (37) for $\Delta\boldsymbol{\Pi}$.
4: correct the state variables by $\boldsymbol{x}^{(k+1)}=\boldsymbol{x}^{(k)}-\Delta\boldsymbol{x}^{(k)}$.
5: judge whether convergence by $\left\|\Delta\boldsymbol{x}^{(k)}\right\|\le\varepsilon$, If yes, then go to 7; else go to 6.
6: set $k = k + 1$, go to 3.
7: output the optimal solution.

D. Comparion of NRMF and FDMF Methods

In this sub-section, the MF solution method based on NRMF method and the proposed FDMF method are compared. The performance comparisons between them are as follows.

1) The NRMF method has a good convergence rate (quadratic). The Jacobian matrix in NRMF needs to be re-calculated and refactorized in each iteration, which is very time-consuming. The approximation made in the FDMF method generally results in a small increase in the number of iterations. However, the computation effort is significantly reduced since the Jacobian matrix in FDMF needs to be calculated and factorized only in the first iteration. The convergence rate of the proposed FDMF method is linear as compared with the quadratic rate of the NRMF method. In general, the computation efficiency of FDMF method is much higher than that of NRMF method, which has been verified in a large number of simulation experiments.

2) Compared with NRMF method, the proposed FDMF method requires less memory in the process of calculation.

IV. Case Study

A. Test on a Small IES

1) Introduction of Test System

To test the performance of the proposed FDMF method, the simulations with the same network and parameters in [15] are firstly conducted. The topology of the IES is shown in Fig. 1.

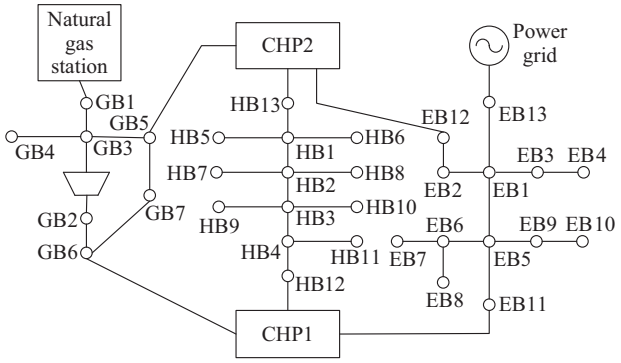

Fig. 1. Structure of test IES.

In Fig. 1, EB*i*, HB*i* and GB*i* denote the electricity node, heat node and natural gas node, respectively. Details can be found in [15]. The algorithm is coded in MATLAB and performed on an Intel(R) Core(TM) i5 PC, 2.40 GHz processor with 8 GB RAM. The convergence accuracy is 10^{-4}.

2) Accuracy Test

1) Test results with original load

With the original load in [15], we have calculated the MF of the above IES system with NRMF method, UMF method proposed in [21] and the proposed FDMF method. Tables I-IV shows the estimates of complex voltage for electricity system, the supply temperature and return temperature as well as the pipeline mass rate for heat system, and the estimates of node pressure for natural gas system, respectively, where No. denotes the number of nodes, Br. denotes the branch number of heat system.

TABLE I
Estimates of Complex Voltage for Electricity System

No.	Voltage (p.u.)			Angle (°)		
	NRMF	UMF	FDMF	NRMF	UMF	FDMF
1	1.0484	1.0484	1.0484	3.1173	3.1173	3.1173
2	1.0460	1.0460	1.0461	2.8477	2.8477	2.8477
3	1.0220	1.0220	1.0220	4.4581	4.4581	4.4581
4	1.0099	1.0099	1.0099	5.1790	5.1790	5.1790
5	1.0187	1.0187	1.0187	5.3422	5.3422	5.3422
6	0.9986	0.9986	0.9986	6.2685	6.2685	6.2685
7	0.9957	0.9957	0.9957	6.4188	6.4188	6.4188
8	0.9959	0.9959	0.9959	–6.3694	–6.3694	–6.3694
9	1.0005	1.0005	1.0005	–5.8714	–5.8714	–5.8714
10	0.9866	0.9866	0.9866	–6.3003	–6.3003	–6.3003
11	1.0500	1.0500	1.0500	–5.2796	–5.2796	–5.2796
12	1.0500	1.0500	1.0500	–2.1312	–2.1312	–2.1312
13	1.0838	1.0838	1.0838	0	0	0

TABLE II
Estimates of Pipeline Mass Rate for Heat System

Br.	Mass rate (kg/s)		
	NRMF	UMF	FDMF
13-1	5.6043	5.6043	5.6043
1-2	2.6826	2.6826	2.6826
2-3	0.7013	0.7013	0.7013
4-3	2.7929	2.7929	2.7929
12-4	4.7346	4.7346	4.7346
1-5	0.9811	0.9811	0.9811
1-6	0.9768	0.9768	0.9768
2-7	0.5037	0.5037	0.5037
2-8	0.5011	0.5011	0.5011
3-9	1.4984	1.4984	1.4984
3-10	1.0027	1.0027	1.0027
4-11	0.9748	0.9748	0.9748

As shown in Tables I-IV, the calculation results given by the NRMF method, the UMF method and the proposed FDMF method are exactly the same. This proves the correctness of the proposed FDMF method in this paper.

TABLE III
ESTIMATES OF SUPPLY TEMPERATURE AND RETURN TEMPERATURE FOR HEAT SYSTEM

No.	Supply temperature (℃)			Return temperature (℃)		
	NRMF	UMF	FDMF	NRMF	UMF	FDMF
1	99.6168	99.6168	99.6168	49.4211	49.4211	49.4211
2	98.9800	98.9800	98.9800	49.3185	49.3185	49.3185
3	98.1566	98.1566	98.1566	49.8853	49.8853	49.8853
4	99.4562	99.4562	99.4562	49.7354	49.7354	49.7354
5	98.7473	98.7473	98.7473	50.0000	50.0000	50.0000
6	98.9611	98.9611	98.9611	50.0000	50.0000	50.0000
7	97.4723	97.4723	97.4723	50.0000	50.0000	50.0000
8	97.7154	97.7154	97.7154	50.0000	50.0000	50.0000
9	97.8757	97.8757	97.8757	50.0000	50.0000	50.0000
10	97.6953	97.6953	97.6953	50.0000	50.0000	50.0000
11	99.0621	99.0621	99.0621	50.0000	50.0000	50.0000
12	100.0000	100.0000	100.0000	49.4954	49.4954	49.4954
13	100.0000	100.0000	100.0000	49.2533	49.2533	49.2533

TABLE IV
ESTIMATES OF NODE PRESSURE FOR NATURAL GAS SYSTEM

No.	Pressure (bar)		
	NRMF	UMF	FDMF
1	5.0000	5.0000	5.0000
2	5.0000	5.0000	5.0000
3	4.4973	4.4973	4.4973
4	4.4839	4.4839	4.4839
5	4.4397	4.4397	4.4397
6	4.4394	4.4394	4.4394
7	4.4323	4.4323	4.4323

At the same time, it can be found that Jacobian matrix has the following characteristics in the estimation process: ① during the iteration process, the values of $\boldsymbol{C}_s$ and $\boldsymbol{C}_r$ do not change much, which verifies the correctness of the model (35); ② during the iteration process, the Jacobian matrix of FDMF is indeed close to the constant diagonal matrix, which further proves the correctness of the proposed FDMF method; ③ the largest element in $\boldsymbol{J}_{h21}$ in this case does not exceed 10^{-3}, and most of the elements in $\boldsymbol{J}_{h21}$ are close to 10^{-4}, as a result, $\boldsymbol{J}_{h21}$ can be considered as null matrix in the calculation.

2) Test results with increased load

For more tests, we have changed the boundary conditions of the same system in Fig. 1 by increasing the load. Specifically, the loads of nodes 3 and 4 in the heat system are increased to 0.25 MW. Before and after loads increase, the supply temperatures of all the nodes in the heat system with NRMF and FDMF methods are shown in Fig. 2.

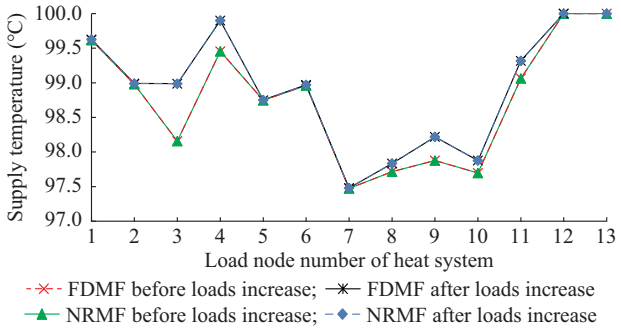

Fig. 2. Supply temperatures of all the nodes in heat system with NRMF and FDMF methods.

As shown in Fig. 2, whether before or after loads increase, the supply temperatures of all the nodes in the heat system with FDMF method are equal to those with NRMF method, thereby demonstrating the correctness of FDMF method regardless of the IES operation state.

3) Test of Computation Efficiency

1) Flat-start is used as initial points

The computation efficiency of NRMF method, UMF method in [21] and the proposed FDMF method are also tested. They are firstly tested with the original load, then all the electrical, heat and natural gas loads are gradually increased by 2% each time. In all tests, flat-start is used as the initial points and the results obtained by the three methods are the same. The average number of iterations and the average calculation time of the above three methods under different load levels in 1000 experiments are shown in Table V, where computation efficiency ratio denotes the ratio of the computation efficiency of FDMF to that of NRMF.

TABLE V
AVERAGE NUMBER OF ITERATIONS AND CPU TIME UNDER DIFFERENT LOAD LEVELS

Load level	Iteration count			CPU time (s)			Computation efficiency ratio
	NRMF	UMF	FDMF	NRMF	UMF	FDMF	
Original load	7	7	11	11.5800	10.1200	2.7278	4.2452
Load increased by 2%	7	7	11	11.5800	10.1200	2.7278	4.2452
Load increased by 4%	7	7	11	11.5800	10.1200	2.7278	4.2452
Load increased by 6%	7	7	11	11.5801	10.1202	2.7278	4.2452
Load increased by 8%	7	7	11	11.5801	10.1205	2.7278	4.2452
Load increased by 10%	7	7	11	11.5802	10.1205	2.7278	4.2452

As shown in Table V, with the original load, the NRMF method needs 7 iterations to converge, and the average calculation time is about 11.58 s. Whereas the FDMF method needs 11 iterations to converge, and the average calculation time is about 2.7278 s. Among all the tests, the calculation efficiency of the proposed FDMF method is the highest, fol-

lowed by UMF method, and that of NRMF method is the lowest.

With the gradual increase of all load levels step by step, the computation efficiency of NRMF method, UMF method and FDMF method basically remains unchanged. At all load levels, the computation efficiency of FDMF method is more than four times that of NRMF. This is due to the fact that in the iteration process of the FDMF method, the Jacobian matrix only needs to be calculated and factorized in the first iteration. Whereas in the iteration process of the NRMF method, the Jacobian matrix needs to be reconstructed and refactorized in each iteration. The test results demonstrate that the proposed FDMF method has better computation efficiency than the existing NRMF method.

2) Other initial points used

We further test the effects of different initial points on the performances of NRMF and FDMF methods. In the tests, we gradually shift the initial points from the flat start points, and then test NRMF and FDMF. The test results are shown in Table VI.

TABLE VI
AVERAGE NUMBER OF ITERATIONS AND CPU TIME OF DIFFERENT INITIAL POINTS

Initial point	Iteration count		CPU time (s)		Computation efficiency ratio
	NRMF	FDMF	NRMF	FDMF	
Flat start point	7	11	11.5800	2.7278	4.2452
Flat start point increased by 2%	7	11	11.5800	2.7278	4.2452
Flat start point increased by 4%	8	11	13.2343	2.7278	4.8516
Flat start point increased by 6%	8	11	13.2343	2.7278	4.8516
Flat start point increased by 8%	9	11	14.8885	2.7278	5.4581
Flat start point increased by 10%	10	11	16.5429	2.7278	6.0646

As shown in Table VI, with the initial points gradually deviating from the flat start points, the convergence of NRMF method becomes worse while that of the proposed FDMF method remains unchanged, which proves that compared with NRMF, the FDMF method is less sensitive to the initial points.

B. Test on a Large IES

To further test the performance of the proposed method, a large IES with 4 small IESs connected with IEEE-118 bus system is constructed as shown in Appendix A Fig. A1. This large IES consists of 170 power nodes, 52 heat nodes, 28 natural gas nodes and 8 CHPs. The parameters of the 4 small IESs are the same as those in the system of Fig. 1.

The MFs of the large IES with NRMF method, UMF method [21] and the proposed FDMF method are calculated. The estimation values of state variables obtained by the above three methods are exactly the same. The comparisons of computation efficiency are shown in Table VII, where the computation efficiency ratio denotes the ratio of the computation efficiency of FDMF to that of NRMF.

TABLE VII
AVERAGE NUMBER OF ITERATIONS AND CPU TIME IN LARGE IES

Load level	Iterations			CPU time (s)			Computation efficiency ratio
	NRMF	UMF	FDMF	NRMF	UMF	FDMF	
Original load	8	8	11	59.5441	58.1339	11.7295	5.0764
Load increased by 2%	8	8	11	59.5441	58.1339	11.7295	5.0764
Load increased by 4%	8	8	11	59.5441	58.1339	11.7295	5.0764
Load increased by 6%	8	8	11	59.5441	58.1339	11.7295	5.0764
Load increased by 8%	8	8	11	59.5441	58.1339	11.7295	5.0764
Load increased by 10%	8	8	11	59.5442	58.1340	11.7295	5.0764

The maximum error of state variables obtained by the proposed FDMF method and the NRMF method is no more than 10^{-4}. This proves that the FDMF method proposed in this paper is still correct for large IES.

As shown in Table VII, in this large IES, the calculation efficiency of the proposed FDMF method is still the highest, followed by UMF method, and the calculation efficiency of NRMF method is the lowest. Compared with that of NRMF method, it can be concluded that the larger the system is, the more efficient the calculation of FDMF method is. Since that Jacobian matrix of the NRMF method will be sparser for large IES, much computation is redundant in the NRMF method. At this time, the proposed FDMF method is more adaptable and has higher computation efficiency.

V. CONCLUSION

In this paper, an FDMF calculation method for IES is proposed through replacing the original Jacobian matrix of MF calculation based on NRMF method with a diagonal and constant Jacobian matrix by the transformation. Detailed theoretical derivation and modeling process are given. Test cases on IES systems demonstrate that the proposed FDMF meth-

od possesses good convergence and high computation efficiency.

APPENDIX A

The topology of a large-scale IES is shown in Fig. A1.

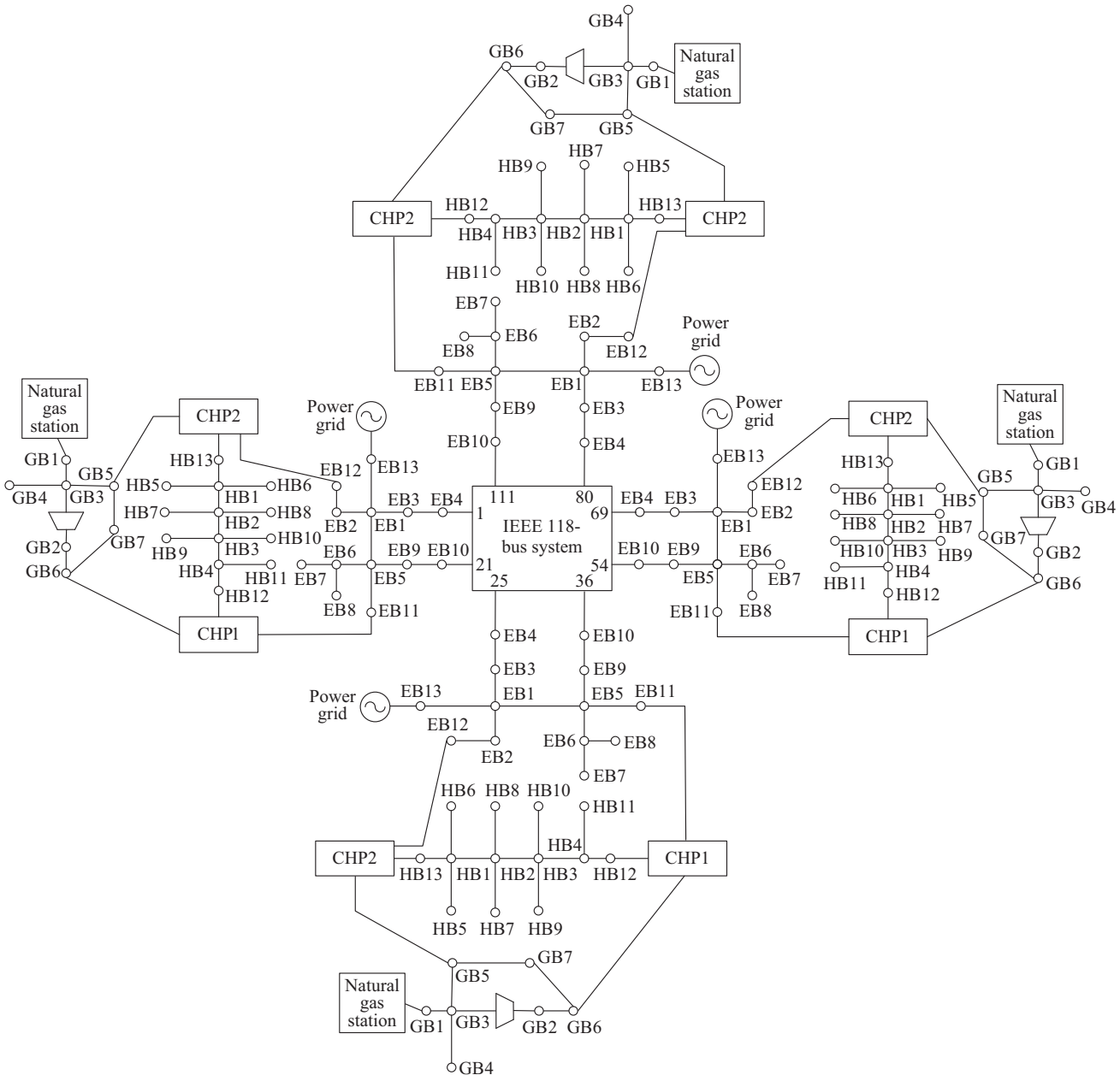

Fig. A1. Topology of a large-scale IES.

REFERENCES

[1] X. Liu, J. Wu, N. Jenkins *et al*., "Combined analysis of electricity and heat networks," *Applied Energy*, vol. 162, pp. 1238-1250, Jan. 2016.

[2] M. T. Rees, J. Wu, N. Jenkins *et al*., "Carbon constrained design of energy infrastructure for new build schemes," *Applied Energy*, vol. 113, pp. 1220-1234, Jan. 2014.

[3] B. Awad, M. Chaudry, J. Wu *et al*., "Integrated optimal power flow for electric power and heat in a microgrid," in *Proceedings of the 20th International Conference and Exhibition on Electricity Distribution*, Prague, Czech Republic, Jun. 2009, pp. 1-4.

[4] X. Zhou, C. Guo, Y. Wang *et al*., "Optimal expansion co-planning of reconfigurable electricity and natural gas distribution systems incorporating energy hubs," *Energies*, vol. 10, no. 1, pp. 1-22, Jan. 2017.

[5] S. An, Q. Li, and T. W. Gedra, "Natural gas and electricity optimal power flow," in *Proceedings of IEEE PES Transmission and Distribution Conference and Exposition*, Dallas, USA, Sept. 2003, pp. 138-143.

[6] M. Chaudry, N. Jenkins, and G. Strbac, "Multi-time period combined gas and electricity network optimisation," *Electric Power Systems Research*, vol. 78, no. 7, pp. 1265-1279, Jul. 2008.

[7] A. Martinez-Mares and C. R. Fuerte-Esquivel, "A unified gas and power flow analysis in natural gas and electricity coupled networks," *IEEE Transactions on Power Systems*, vol. 27, no. 4, pp. 2156-2166, Nov. 2012.

[8] R. Rubio-Barros, D. Ojeda-Esteybar, A. Vargas *et al*., "Energy carrier networks: interactions and integrated operational planning," in *Handbook of Networks in Power Systems II*. Berlin: Springer, 2012, pp. 117-167.

[9] Y. Zhang, "Study on analytical method of natural gas - electric power mixing system," Ph.D. dissertation, China Electric Power Research Institute, Beijing, China, 2005.

[10] P. Liu, D. I. Gerogiorgis, and E. N. Pistikopoulos, "Modeling and opti-

mization of polygeneration energy systems," *Catalysis Today*, vol. 127, no. 1, pp. 347-359, Sept. 2007.
[11] C. Wang, B. Hong, and L. Guo, "A general modeling method for optimal dispatch of combined cooling, heating and power microgrid," *Proceedings of the CSEE*, vol. 33, no. 31, pp. 26-33, Nov. 2013.
[12] R. Wang, W. Gu, and Z. Wu, "Economic and optimal operation of a combined heat and power microgrid with renewable energy resources," *Automation of Electric Power Systems*, vol. 35, no. 8, pp. 22-27, Apr. 2011.
[13] M. Geidl and G. Andersson, "Optimal power flow of multiple energy carriers," *IEEE Transaction on Power Systems*, vol. 22, no. 1, pp. 145-155, Feb. 2007.
[14] M. Arnold, R. R. Negenborn, G. Andersson *et al*., "Distributed control applied to combined electricity and natural gas infrastructures," in *Proceedings of International Conference on Infrastructure Systems and Services: Building Networks for a Brighter Future (INFRA)*, Rotterdam, Netherlands, Nov. 2008, pp. 1-6.
[15] Y. Wang, B. Zeng, J. Guo *et al*., "Multi-energy flow calculation method for integrated energy system containing electricity, heat and gas," *Power System Technology*, vol. 40, no. 10, pp. 2942-2950, Oct. 2016.
[16] X, Xu, H. Jia, X. Jin *et al*., "Study on hybrid heat-gas-power flow algorithm for integrated community energy system," *Proceedings of the CSEE*, vol. 35, no. 14, pp. 3634-3642, Jul. 2015.
[17] Z. Pan, Q. Guo, and H. Sun, "Interactions of district electricity and heating systems considering time-scale characteristics based on quasi-steady multi-energy flow," *Applied Energy*, vol. 167, pp. 230-243, Apr. 2016.
[18] M. Moeini-Aghtaie, A. Abbaspour, M. Fotuhi-Firuzabad *et al*., "A decomposed solution to multiple-energy carriers optimal power flow," *IEEE Transactions on Power Systems*, vol. 29, no. 2, pp. 707-716, Mar. 2014.
[19] A. Shabanpour-Haghighi and A. R. Seifi, "Simultaneous integrated optimal energy flow of electricity, gas, and heat," *Energy Conversion and Management*, vol. 101, pp. 579-591, Sept. 2015.
[20] X. Liu and P. Mancarella, "Modelling, assessment and Sankey diagrams of integrated electricity-heat-gas networks in multi-vector district energy systems," *Applied Energy*, vol. 167, pp. 336-352, Apr. 2016.
[21] A. Shabanpour-Haghighi and A. R. Seifi, "An integrated steady-state operation assessment of electrical, natural gas, and district heating networks," *IEEE Transactions on Power Systems*, vol. 31, no. 5, pp. 3636-3647, Sept. 2016.
[22] W. Lin and J. Teng, "Three-phase distribution network fast-decoupled power flow solutions," *International Journal of Electrical Power & Energy Systems*, vol. 22, no. 5, pp. 375-380, Jun. 2000.
[23] P. Aravindhababu, "A new fast decoupled power flow method for distribution systems," *Electric Power Components and Systems*, vol. 36, no. 9, pp. 869-878, Jun. 2010.
[24] X. Li, F. Li, H. Yuan *et al*., "GPU-based fast decoupled power flow with preconditioned iterative solver and inexact Newton method," *IEEE Transactions on Power Systems*, vol. 32, no. 4, pp. 2695-2703, Jul. 2017.
[25] Y. Chen, Z. Zhang, H. Fang *et al*., "Generalised-fast decoupled state estimator," *IET Generation, Transmission & Distribution*, vol. 12, no. 22, pp. 5928-5938, Sept. 2018.

Yanbo Chen received the B.S., the M.S., and the Ph.D. degrees in electrical engineering from Huazhong University of Science and Technology, Wuhan, China, China Electric Power Research Institute, Beijing, China, and Tsinghua University, Beijing, China, in 2007, 2010 and 2013, respectively. He is currently an Associate Professor of North China Electric Power University, Beijing, China. His research interests include state estimation, power system analysis and control, and integrated energy system.

Junyuan Zhao received the B. S. degree in electrical engineering from North China Electric Power University, Beijing, China, in 2018. She is currently pursuing the M.S. degree in electrical engineering at McGill University, Québec, Canada. Her research interests include power system, integrated energy system and smart grid.

Jin Ma received the B.S. and M.S. degrees in electrical engineering from Zhejiang University, Hangzhou, China, the Ph.D. degree in electrical engineering from Tsinghua University, Beijing, China, in 1997, 2000, and 2004, respectively. He is currently with the School of Electrical and Information Engineering, University of Sydney, Sydney, Australia. He is the member of CIGRE W.G. C4.605 and the corresponding member of CIGRE Joint Workgroup C4-C6/CIRED. He is a registered Chartered Engineer. His research interests include load modeling, nonlinear control system, dynamic power system, and power system economics.